# A quantitative proteomic analysis of cofilin phosphorylation in myeloid cells and its modulation using the LIM kinase inhibitor Pyr1

Renaud Prudent[1], Nathalie Demoncheaux[1], Hélène Diemer[2], Véronique Collin-Faure[3], Reuben Kapur[4], Fabrice Paublant[1], Laurence Lafanechère[5]*, Sarah Cianférani[2☉], Thierry Rabilloud☉[3☉]*

1 CELLIPSE SAS, Grenoble, France, 2 Laboratoire de Spectrométrie de Masse BioOrganique (LSMBO), Université de Strasbourg, CNRS, IPHC UMR 7178, Strasbourg, France, 3 Chemistry and Biology of Metals, Univ. Grenoble Alpes, CNRS UMR5249, CEA, BIG-LCBM, Grenoble, France, 4 Department of Pediatrics, Herman B Wells Center for Pediatric Research, Indiana University School of Medicine, Indianapolis, United States of America, 5 Institute for Advanced Biosciences, Univ. Grenoble Alpes, CNRS UMR 5309, INSERM U1209; Grenoble, France

☉ These authors contributed equally to this work.
* thierry.rabilloud@cea.fr (TR); laurence.lafanechere@univ-grenoble-alpes.fr (LL)

Check for updates

🔓 OPEN ACCESS

## Abstract

LIM kinases are located at a strategic crossroad, downstream of several signaling pathways and upstream of effectors such as microtubules and the actin cytoskeleton. Cofilin is the only LIM kinases substrate that is well described to date, and its phosphorylation on serine 3 by LIM kinases controls cofilin actin-severing activity. Consequently, LIM kinases inhibition leads to actin cytoskeleton disorganization and blockade of cell motility, which makes this strategy attractive in anticancer treatments. LIMK has also been reported to be involved in pathways that are deregulated in hematologic malignancies, with little information regarding cofilin phosphorylation status. We have used proteomic approaches to investigate quantitatively and in detail the phosphorylation status of cofilin in myeloid tumor cell lines of murine and human origin. Our results show that under standard conditions, only a small fraction (10 to 30% depending on the cell line) of cofilin is phosphorylated (including serine 3 phosphorylation). In addition, after a pharmacological inhibition of LIM kinases, a residual cofilin phosphorylation is observed on serine 3. Interestingly, this 2D gel based proteomic study identified new phosphorylation sites on cofilin, such as threonine 63, tyrosine 82 and serine 108.

## Introduction

Targeting cytoskeletal components, such as actin or tubulin has been shown to inhibit the invasive and metastatic behavior of cancer cells [1, 2]. Pharmacological agents targeting the cytoskeleton are however toxic for many proliferating normal cells as well as peripheral neurons, inducing severe adverse effects. Novel alternative pharmacological strategies aim at

targeting cytoskeleton-regulating proteins, which are selectively deregulated during cancer progression. LIM kinases (LIMK), a family of two highly related members, LIMK1 and LIMK2, which control both actin and microtubule dynamics [3] and are overexpressed in many invasive cancers, are an attractive target [4, 5].

The initially- and most extensively- described substrates of LIMK are members of the actin-depolymerizing factor (ADF)/cofilin family of actin-binding proteins (Cofilin1, cofilin 2 and ADF), which control actin cytoskeleton dynamics [6].

LIM kinases phosphorylate cofilin on serine 3 [7], which leads to cofilin inactivation, resulting in reorganisation of the actin cytoskeleton. In adherent cells LIMK increases stress fibre and focal adhesion formation by reducing actin depolymerisation. LIMK-initiated changes in F-actin severing also leads to reduced barbed end formation and leading edge protrusions.

An overexpression of LIMK is observed in many invasive cancers, which could be associated with increased EMT [8] and motility acquisition by metastatic cells.

Upon LIMK inhibition, microtubules are stabilized and actin filaments are disorganized [3, 9,10]. Western blotting with phospho-S3 cofilin-specific antibodies, show in most cases a strong decrease of S3 phosphorylation [9–14]. Recent findings indicate that pharmacological inhibition of LIMK has a strong effect on the growth and invasive behavior of breast cancer cells in 3D cell models [15] and in animal tumor models [16]. Such a treatment was well-tolerated and showed efficacy even on taxane resistant tumors [16].

Recent data also indicate that inhibition of LIMK may also be of interest in hematologic malignancies, where overexpression of a signaling pathway involving LIMK is observed [17, 18]. Several reports suggest that targeting LIMK [19] in leukemia may be of therapeutic value. Especially, it has been evidenced that inhibiting LIMK exerts an anti-leukemic activity in murine model of leukemia [10].

With the ultimate goal of better understanding the role of LIMK and the dynamic regulation of the cytoskeleton in the functions of these non-epithelial cell types, we first analyzed in depth the phosphorylation of cofilin and studied how it was impacted by inhibition of LIMK using the well-described Pyr1 inhibitor [3]. Since the WB technique is only grossly quantitative [20–23], we analyzed the degree of cofilin phosphorylation by phospho-proteomics.

This approach made it possible to demonstrate that in these cell types, under our experimental conditions, a residual phosphorylation of cofilin can be o bserved on serine 3 after pharmacological inhibition of LIMK. In addition, we have identified new phosphorylated sites. Since Ser 3 cofilin is the main site of actin severing regulation and considering the phylogenic conservation of these new sites, it is likely that multiples regulations of cofilin are yet to be discovered.

## Material and methods

### Chemical reagent

Pyr1 was synthetized as described in [10].To maximize its effect it was used at 25 μM, its maximal soluble concentration in most cell culture media. Pyr-1 was prepared as a concentrated solution in DMSO, and an amount of DMSO equal to the one that is contained in the 25 M Pyr1 solution was added to the control cultures.

### Cell lines and cell culture

MV4-11 and Kasumi-1 cell lines were originally purchased from the American Type Culture Collection (ATCC). MV4-11and Kasumi-1 cells were cultured in RPMI 1640 10% (v/v) fetal bovine serum FBS supplemented with 100 U/ml penicillin, 0.1mg/ml streptomycin (PAN Biotech P06-07100) and 2mM Glutamine (Sigma-Aldrich 59202C). Murine IL-3-dependent

myeloid cell line 32D cells bearing MIEG3 vector, KIT WT or KITD814V mutant were cultured in medium containing IMDM supplemented with 10% FBS and murine IL-3 (10 ng/ml). Cells were maintained at 37˚C with 5% $CO_2$. For treatment with Pyr1, cells were treated for 2 hours with 25 μM Pyr1 or with DMSO.

For the cell proliferation assay, cells were seeded in 96 wells microplates at 5,000 cells per well (MV 4–11, 32D-WT and 32D-D814V cell lines) or at 20,000 cells per well (Kasumi-1 cell line). Compounds (or equivalent amounts of DMSO) were then added and cells were allowed to grow for 48 hours (MV4-11, 32D-WT and 32D-D814V cell lines) or 96 hours (Kasumi-1cell line). Proliferation was evaluated using PrestoBlue assay according to manufacturer recommendations. Results are expressed as GI50 (Growth Inhibition 50%), TGI (Total Growth Inhibition) and LD50 (Letal Dose 50%) in comparison to DMSO controls.

## Proteomics

The 2D gel based proteomic experiments were essentially carried out as previously described [24]. However, detailed material and methods are provided for the sake of paper consistency and for phosphopeptide identification and quantification.

**Sample preparation.** The cells were collected, and then washed three times in PBS. The cells were then washed once in TSE buffer (10 mM Tris-HCl pH 7.5, 0.25M sucrose, 1mM EDTA), and the volume of the cell pellet was estimated. The pellet was resuspended in its own volume of TSE buffer. Then 4 volumes (respective to the cell suspension just prepared) of concentrated lysis buffer (8.75 M urea, 2.5 M thiourea, 5% (w/v) CHAPS, 6.25 mM TCEP-HCl, 12.5 mM spermine base, 25 mM HCl) were added and the solution was let to extract at room temperature for 1 hour. The nucleic acids were then pelleted by centrifugation (15,000 g at room temperature for 15 minutes), and the protein concentration in the supernatant was determined by a dye-binding assay [25]. Carrier ampholytes (Pharmalytes pH 3–10) were added to a final concentration of 0.4% (w/v), and the samples were kept frozen at -20˚C until use.

**Isoelectric focusing.** Home-made 160 mm long 4–8 linear pH gradient gels [26] cast according to published procedures [27] or commercial non linear 3–10, 18 cm long pH gradients (Serva) were used. In the former case, four mm-wide strips were cut. The strips were rehydrated overnight with the sample, diluted in a final volume of 0.6 ml of rehydration solution (7M urea, 2M thiourea, 4% (w/v) CHAPS, 0.4% carrier ampholytes (Pharmalytes 3–10) and 100mM dithiodiethanol [28] for the 4 mm-wide strips and in 0.35 ml of rehydration solution for the commercial strips.

The strips were then placed in a Multiphor plate (GE Healthcare), and IEF was carried out with the following electrical parameters: 100V for 1 hour, then 300V for 3 hours, then 1000V for 1 hour, then 3400 V up to 60–70 kVh. After IEF, the gels were equilibrated for 20 minutes in 125mM Tris, 100mM HCl, 2.5% SDS, 30% (v/v) glycerol and 6M urea [29]. They were then transferred on top of the SDS gels and sealed in place with 1% agarose dissolved in Tris 125mM, HCl 100mM, SDS 0.4% and 0.005% (w/v) bromophenol blue.

**SDS electrophoresis and protein detection.** Ten percent gels (160x200x1.5 mm) were used for protein separation. The Tris taurine buffer system [30] was used and operated at a ionic strength of 0.1 and a pH of 7.9. The final gel composition was thus 180mM Tris, 100 mM HCl, 10% (w/v) acrylamide, 0.27% bisacrylamide. The upper electrode buffer was 50 mM Tris, 200 mM taurine, 0.1% SDS. The lower electrode buffer was 50 mM Tris, 200 mM glycine, 0.1% SDS. The gels were run at 25V for 1hour, then 12.5W per gel until the dye front has reached the bottom of the gel. Detection was carried out by a tetrathionate silver staining [31].

**Blotting.** When blotting was performed, 2D gels were used immediately after the second dimension migration. Proteins were transferred on PVDF membranes using the semidry blotting

system of Kyhse-Andersen,[32] with some of the modifications introduced by Laurière [33]. Briefly, the anode buffers, including the PVDF-impregnating buffer contained 20% ethanol (v/v), while the cathode buffer contained 0.1% SDS (w/v). The electrophoretic transfer proceeded at 0.8 mA/cm2 of membrane. After transfer, the blot was first stained overnight with india ink, and then submitted to immunodetection [34], with all steps performed at room temperature. To this purpose, the PVDF membrane (Merck-Millipore Immobilon P IPVH00010) is blocked with Tris Buffered Saline, pH 7.4 (TBS) with 0.1% Tween 20 and 5% BSA for 1h under agitation. The membrane was rinsed 3 times 10min under agitation with TBS, 0.1% Tween-20 (TBST) and then 1hour with anti-phospho-Ser3-cofilin (Cell Signaling Technology #3313, 1/1000 dilution) antibody or anti-cofilin (Cell Signaling Technology #3312, 1/1000 dilution) antibody diluted in TBS, 0.1% Tween 20 and 1% BSA. The membrane is then rinsed 3 times 10min under agitation in TBST and incubated for 1 hour with anti-rabbit secondary antibody, horseradish peroxidase conjugated (Jackson Immunoresearch #711-036-152) under agitation. After three washes (10min each) in TBST, the detection of total or phosphorylated cofilin was performed using chemiluminescence kit ECL Plus (GE Healthcare RPN2132). The signal was acquired on a C-Digit model 3600 (Licor).

**Image analysis.** The gels were scanned after silver staining on a flatbed scanner (Epson perfection V750), using a 16 bits grayscale image acquisition. The gel images were then analyzed using the Delta 2D software (v 4.1). The spots intensities were normalized by the software as the fraction (in percent) of the sum of all detected spots. This allowed the quantitative comparison of the various cofilin spots in all gels analyzed.

For determining the effects of LIMK inhibition on cofilin phosphorylation, statistical tests were used. As different culture batches can show quantitatively different 2D gel profiles, paired (by culture batch) and unpaired (over the complete replicate series) T-tests were used.

**Mass spectrometry.** The spots selected for identification were excised from silver-stained gels and destained with ferricyanide/thiosulfate on the same day as silver staining in order to improve the efficiency of the identification process [35] [36]. In gel digestion was performed with an automated protein digestion system, MassPrep Station (Waters, Milford, USA). The gel plugs were washed twice with 50 µL of 25 mM ammonium hydrogen carbonate ($NH_4HCO_3$) and 50 µL of acetonitrile. The cysteine residues were reduced by 50 µL of 10 mM dithiothreitol at 57°C and alkylated by 50 µL of 55 mM iodoacetamide. After dehydration with acetonitrile, the proteins were cleaved in gel with 10 µL of 7 ng/µL of modified porcine trypsin (Promega, Madison, WI, USA) in 25 mM $NH_4HCO_3$. The digestion was performed overnight at room temperature. The generated peptides were extracted with 40 µL of 60% acetonitrile in 0.1% formic acid. Acetonitrile was evaporated under vacuum before nanoLC-MS/MS analysis.

NanoLC-MS/MS analysis was performed using a nanoACQUITY Ultra-High-Performance-LC (Waters Corporation, Milford, USA) coupled to the TripleTOF 5600 (Sciex, Ontario, Canada).

The nanoLC system was composed of ACQUITY UPLC CSH130 C18 column (250 mm x 75 µm with a 1.7 µm particle size, Waters Corporation, Milford, USA) and a Symmetry C18 precolumn (20 mm × 180 µm with a 5 µm particle size, Waters Corporation, Milford, USA). The solvent system consisted of 0.1% formic acid in water (solvent A) and 0.1% formic acid in acetonitrile (solvent B). 4 µL of sample were loaded into the enrichment column during 3 min at 5 µL/min with 99% of solvent A and 1% of solvent B. Elution of the peptides was performed at a flow rate of 300 nL/min with a 8–35% linear gradient of solvent B in 9 minutes.

The TripleTOF 5600 (Sciex, Ontario, Canada) was operated in positive mode, with the following settings: ion spray voltage floating (ISVF) 2300 V, curtain gas (CUR) 10, interface heater temperature (IHT) 150, ion source gas 1 (GS1) 2, declustering potential (DP) 80 V. Data-Dependent Acquisition was performed using the Information-Dependent Acquisition

(IDA) mode with Top 10 MS/MS scans. The MS scan had an accumulation time of 250 ms on m/z [400;1250] range and the MS/MS scans 100 ms on m/z [150;1800] range in high sensitivity mode. Switching criteria were set to ions with charge state of 2+ - 4+ and an abundance threshold of more than 500 counts, exclusion time was set at 4 s. IDA rolling collision energy script was used for automatically adapting the CE. Mass calibration of the analyzer was achieved using peptides from digested BSA. The complete system was fully controlled by AnalystTF 1.7 (Sciex). Raw data collected were processed and converted with MSDataConverter in .mgf peak list format.

For protein identification, the MS/MS data were interpreted using a local Mascot server with MASCOT 2.5.1 algorithm (Matrix Science, London, UK) against UniProtKB/SwissProt (version 2016_05, 551,193 sequences). The research was carried out without taxonomy restrictions. Spectra were searched with a mass tolerance of 15 ppm for MS and 0.05 Da for MS/MS data, allowing a maximum of one trypsin missed cleavage. Carbamidomethylation of cysteine residues, oxidation of methionine residues, acetylation of protein n-terminus and phosphorylation of serine, threonine and tyrosine residues were specified as variable modifications. Protein identifications were validated with at least two peptides with Mascot ion score above 30. The mass spectrometry data have been deposited in PRIDE [37].

For cofilin phosphopeptide quantitative analyses, XIC signals of the all peptides identified in the same spot were extracted using the Skyline software (version 4.1.0.11796). Total areas, corresponding to the sum of the 3 extracted isotopes areas, were used for quantitative analysis, as described by Schilling et al [38].

To compensate for differences in MS ionization efficiencies between phosphorylated and non-phosphorylated peptides, we normalized our data in the following manner: the quantification of a given cofilin phosphopeptide in spot III was estimated as the ratio of intensity of the signal of the targeted cofilin phosphopeptide divided by the sum of the intensities of all detected peptides (phosphorylated + nonphosphorylated) in spot III. Although this ratio per se does not provide an absolute value of the abundance of the phosphopeptide of interest, the ratio of the ratios obtained for the same cofilin phosphopeptide in two different experimental conditions (e.g. control vs Pyr1-treated) was used as an indicator of the relative abundance of the phosphopeptide of interest at constant protein amount (same protein background in the spots to be compared) and is independent from differences in ionization efficiencies between peptides.

## Results

### Determination of Pyr1 effects on cells

The effects of Pyr1 on the cell lines used were first investigated. Using a treatment of 48 hours, the growth inhibitory and lethal doses were determined. The results, displayed in **Table 1**,

**Table 1. Effective Pyr1 concentrations on the different cell lines for a 48 hours treatment.**

| cell line | GI 50 (µM) | LD 50 (µM) |
|---|---|---|
| MV4-11 DSMZ | 1.4 | 17.5 |
| Kasumi-1 | 1.2 | 10.3 |
| 32D c-KIT WT | 0.11 | 14.5 |
| 32D c-KIT D814V | 0.42 | 12.9 |

GI 50: Dose producing a 50% inhibition of cell growth over the treatment time (48 hoursLD 50: Dose producing 50% cell death over the treatment time (48 hours)

https://doi.org/10.1371/journal.pone.0208979.t001

show a moderate toxicity and an efficient growth inhibition of the four cell lines tested. We also verified that even at 25 μM, the two-hours treatment used to analyze the effects of LIMK inhibition did not result in any toxicity.

## Assignment of the cofilin spots on the 2D gel patterns

The assignment of the cofilin spots on the 2D gel patterns was initiated by protein blotting and confirmed by mass spectrometry. After transfer on PVDF, the membranes were probed successively with an anti phospho-S3 antibody and with a polyclonal anti-cofilin antibody. The results, displayed on **Fig 1** (with more details shown on S1 Fig) show that only one acidic spot (Spot III, Fig 1A–1C) was phosphorylated on S3, while three other major spots (Spots I, II and IV Fig 1A and 1B) were detected by blotting and confirmed by mass spectrometry. The basic spots (I and II) made indeed the bulk of the cofilin pool. The identity of the spots was confirmed by mass spectrometry for both human and murine cofilin (**Table 2**). As shown in S1 Fig, extensive spot identification by mass spectrometry was carried out to assign the more acidic spots detected by the antibodies on the blots. We could however not confirm the identity of these acidic spots as cofilin. These spots were thus considered as immunoblotting artefacts.

The silver-stained gels were then used to quantify the various forms on several myeloid cell lines, two from human origin and the 32D cell line from murine origin, with or without a mutation (D814V) of c-kit proto-oncogene. Such a mutation is known to induce imatinib-resistant aggressive leukemia and myeloproliferative disorders [39] [40] through a ROCK-LIMK signaling pathway [18].

As shown on **Fig 2**, the phosphorylated cofilin spot (Spot III) represented a minor percentage of the total cofilin in all the cell lines tested, and varied from one cell line to another.

In the wide pH gradients used for the cofilin spots assignment, the area of the phosphorylated cofilin spot is crowded. This may lead to quantitative errors when a more precise appraisal of the phosphorylated cofilin spot is required.

## LIMK inhibition induces a partial decrease of the phosphorylated cofilin spot

To quantitatively investigate the changes of cofilin phosphorylation brought through LIMK inhibition by Pyr1, we used linear 4–8 pH gradients which allowed a more precise resolution of the phosphorylated cofilin spot area than the wide pH gradients used previously for the cofilin spots assignment. Typical silver-stained 2D images of the cofilin regions are shown on **Fig 3** and the detailed quantitative results are displayed in **Table 3**. An important decrease of the phosphorylated cofilin spot intensity upon Pyr1 treatment was seen in all cases. The decrease was however incomplete, ranging from 1.5fold (MV4-11) to 3fold (32D-D814V)

## Phosphorylation landscape of cofilin and its modification upon LIMK inhibition

In 2D gel electrophoresis, all the spots that bear the same number of phosphate groups comigrate. From the observed pI of the spot (Spot I on Fig 3) and from the blotting data (Spot III on Fig 1), it can be deduced that the phosphorylated spot decreased in intensity upon Pyr1 treatment is doubly modified, e.g. N-terminal acetylated (as most eukaryotic cytosolic proteins are) and mono-phosphorylated. To explore the modification landscape of this cofilin spot, we allowed acetylation and phosphorylation as variable modifications and allowed semi-tryptic peptides and one missed-cleavage during the computer analysis of the mass spectrometry data.
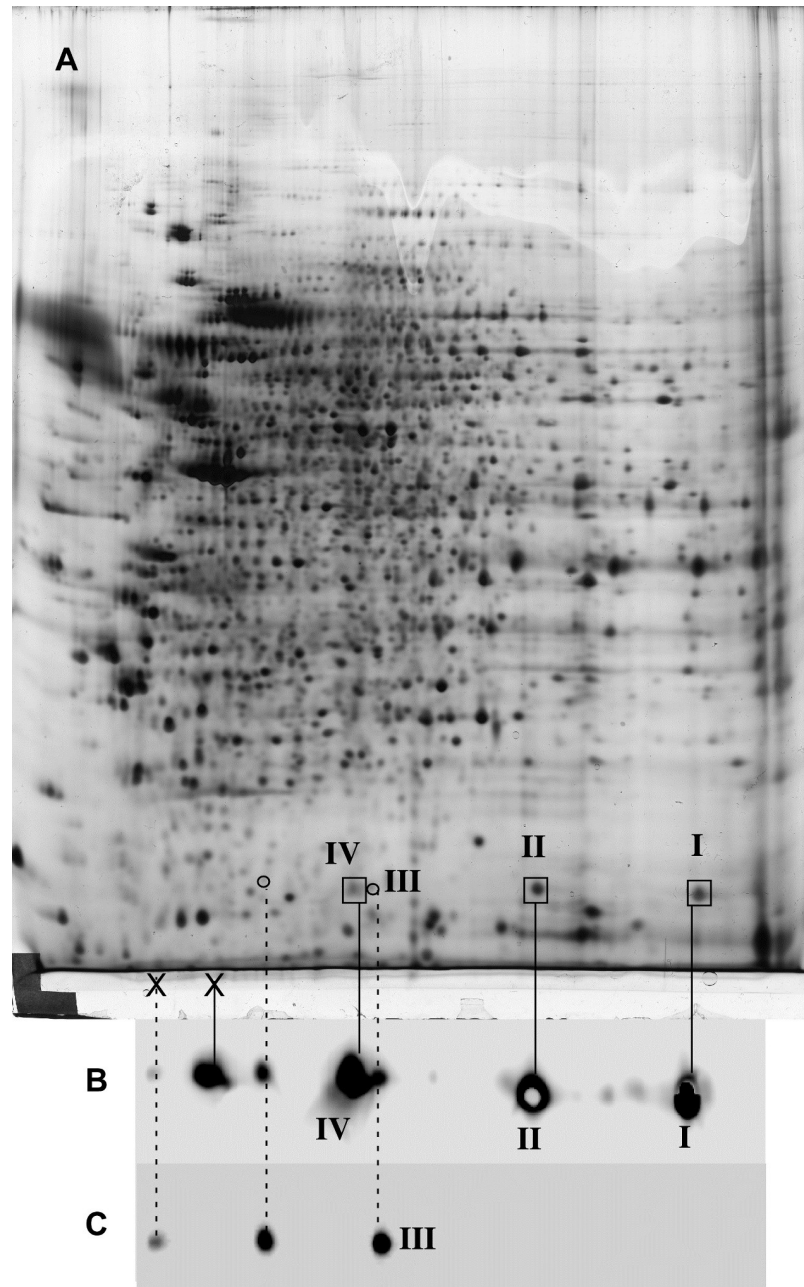
**Fig 1. Alignment of cofilin spots.** The process of alignment and detection of cofilin and phosphocofilin spots has been carried out on the 32D c-kit WT cell line. Proteins were separated on a commercial non linear 3–10 pH gradient. A: silver stained pattern of total proteins. B: western blotting of cofilin spots (I, II, III,IV) with a polyclonal anti-cofilin antibody. C: western blotting of phospho-cofilin spot (III) with an anti phospho S3 peptide antibody The spots labelled with an X correspond to spots that are detected by the antibodies but that could not be confirmed by mass spectrometry.

This resulted in the identification of several modified peptides, including the expected modified N-terminal peptide (N-terminal methionine removed, alanine-2 acetylated and serine-3 phosphorylated), but also the non-phosphorylated form of this N-terminal acetylated peptide. Several additional phosphorylation sites were pointed out by this analysis, on T63, Y82, S108

**Table 2. Spot identification by mass spectrometryT.**

| Cell line | spot | Protein name | Protein accession numbers | Protein molecular weight (Da) | Exclusive unique peptide count | Percentage sequence coverage |
|---|---|---|---|---|---|---|
| Kasumi | IV | Cofilin-1 OS = Homo sapiens | P23528 | 18 503,2 | 12 | 51% |
| | III | Cofilin-1 OS = Homo sapiens | P23528 | 18 503,2 | 14 | 54% |
| | II | Cofilin-1 OS = Homo sapiens | P23528 | 18 503,2 | 10 | 54% |
| | I | Cofilin-1 OS = Homo sapiens | P23528 | 18 503,2 | 12 | 61% |
| 32D | IV | Cofilin-1 OS = Mus musculus | P18760 | 18 560,2 | 12 | 65% |
| | III | Cofilin-1 OS = Mus musculus | P18760 | 18 560,2 | 4 | 27% |
| | II | Cofilin-1 OS = Mus musculus | P18760 | 18 560,2 | 19 | 78% |
| | I | Cofilin-1 OS = Mus musculus | P18760 | 18 560,2 | 23 | 84% |
| | X | ARP 2/3 complex subunit 5-like protein OS = Mus musculus | Q9D898 | 16 941,4 | 3 | 20% |

The identity of the cofilin spots for the MV 4–11 and 32D-D814V cell lines was inferred by spot matching on a cell line from the same species, i.e. on the Kasumi cell line for MV 4–11 and on the 32D-WT for the 32D-D814V cell line

https://doi.org/10.1371/journal.pone.0208979.t002

and S 156, of which only the latter has been previously described in the literature [41]. These results are displayed in **S1 Table** and in **Fig 4**. The modified peptides mass spectra are available in the **S2–S7 Figs**.

The detection of other phosphorylation sites prompted us to re-assess the phosphorylation changes induced by the LIMK inhibitor. Indeed, the forms phosphorylated on other sites may induce a basal level in the mono-phosphorylated cofilin spot, thereby artefactually minimizing the decrease induced by LIMK inhibition. To precisely measure the extent of this decrease, we quantitatively compared the signals obtained for each peptide (**S2–S5 Tables**). As the extraction yield may vary for each spot, e.g. due to its abundance [42] and/or to variability in the spot excision process, we renormalized the peptide signals as the fraction of the total peptide intensities measured for each spot, as described in the methods section. This allowed the calculation of a decrease factor for each of the phosphorylated peptides, which is the combination of this proportion of the phosphopeptide for each spot multiplied by the relative spot abundances measured from the 2D gels. This analysis showed that the reduction in S3 phosphorylation induced by Pyr1 treatment is somewhat higher than detected from the sole quantification of the gel spots. It does not exceed, however, a 5-fold reduction (**Table 4**).

## Discussion

ADF/cofilin proteins are considered to be key modulators of actin dynamics in metastasis and invasion of cancer cells [5, 43–46]. The current view of the regulation of the actin severing activity of cofilin is that it is inactivated by its phosphorylation on S3 thanks to LIMK and is reverted to its basal unphosphorylated active state by the phosphatases slingshot 1 (SSH1) and chronophin (see [6, 47] for reviews). Our results indicate that in myeloid cell lines the phosphorylated proportion of cofilin is minor compared to the unphosphorylated, active fraction. This could reflect a difference in actin dynamics of the analyzed cell lines: these cell lines are mainly non adherent and may not need the same amount of actin microfilaments as adherent cell lines. This could also indicate that a part of the cofilin pool is not accessible to phosphorylation. Moreover, we observed that Pyr1 did not completely inhibit S3 cofilin phosphorylation. There are several possible explanations: firstly, depending on the cell line, the membrane permeability could differ, leading to variable intracellular concentrations of Pyr1 and possible incomplete inhibition. Secondly, lower levels of expression or activity of SSH1 or possible subcellular sequestration of phosphorylated
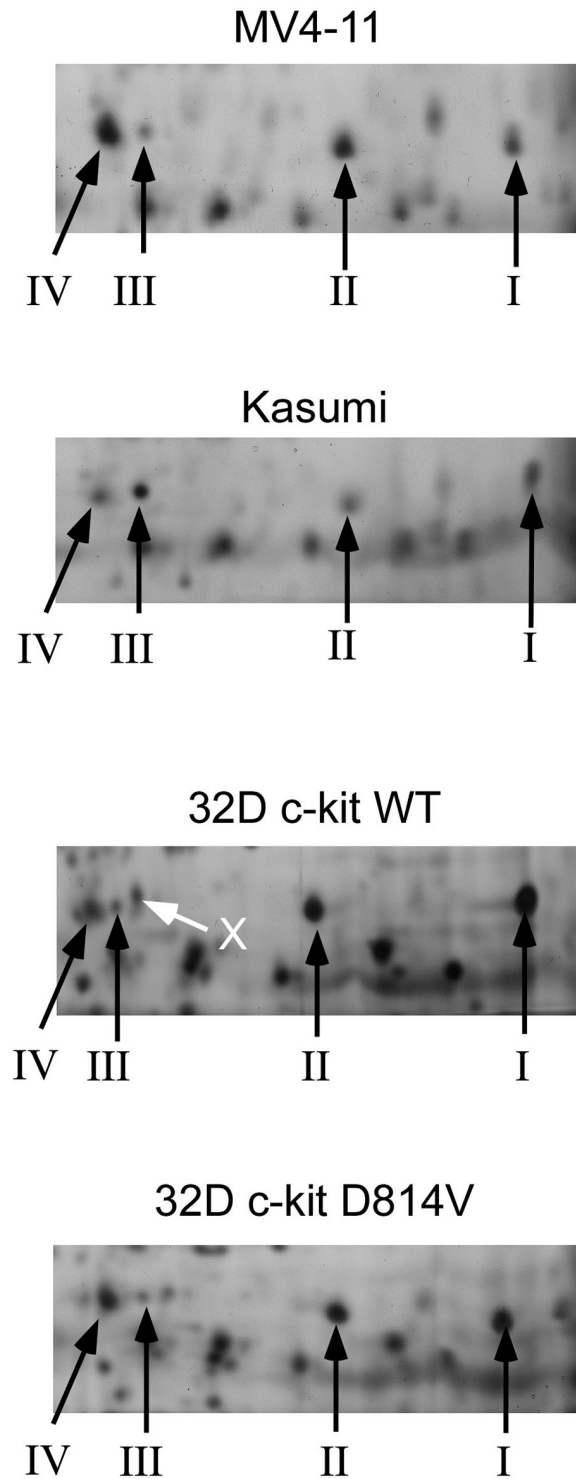
**Fig 2. Cofilin spots profiles of the four cell lines tested.** The areas containing the cofilin spots (I to IV) have been selected for the sake of the clarity of the figure. The protein separation used the same pH gradient as the one used in Fig 1. Note the close vicinity of other protein spots (X) with the phosphocofilin spot (III) in the murine cell lines. In these images, proteins were detected by silver staining.
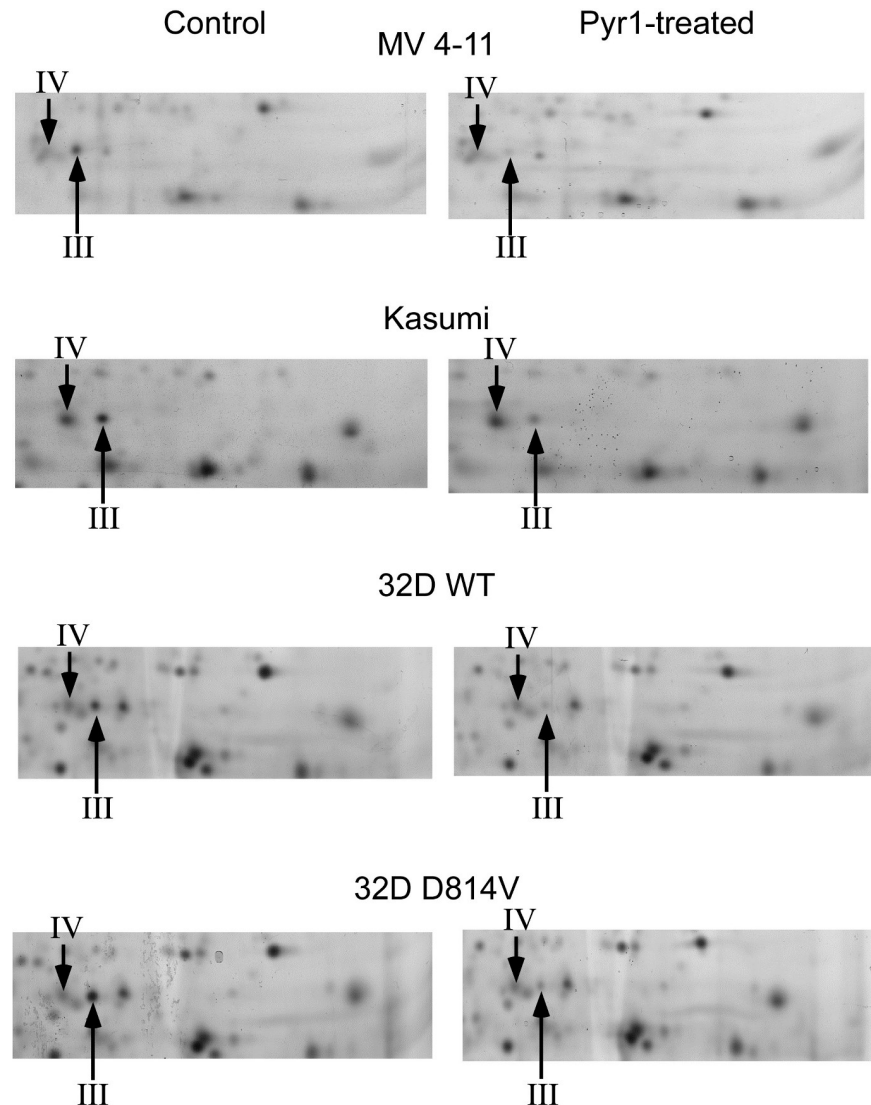
https://doi.org/10.1371/journal.pone.0208979.g002

**Fig 3. Phosphocofilin intensity decrease upon LIMK inhibition.** To reduce the spot crowding around the phosphocofilin spot, a linear 4–8 pH gradient was used. This does not allow the visualization of the basic cofilin spot (spot I), and brings the median spot (II) to the border of the gel, rendering its quantitative measurement unreliable. By contrast, the phosphocofilin spot (III) is more separated from neighboring spots and can be more precisely quantitatively measured. It is also worth noting that spot IV, which is not detected by the anti phospho S3 peptide antibody, does not respond to Pyr-1 treatment. In these images, proteins were detected by silver staining.

cofilin could lead to residual cofilin phosphorylation. Thirdly, it has been shown that other kinases than LIMK are able to phosphorylate cofilin at S3 [48–50]. These Pyr1-insensitive kinases could be responsible of the observed residual cofilin phosphorylation.

A possible similar residual cofilin phosphorylation could also explain why LIMK inhibition did not reduce spontaneous metastasis in animal tumor models [16, 51].

Conversely, the described antitumor effect of LIMK inhibition could involve other subtrates than cofilin. It has been shown that the microtubule cytoskeleton is also impacted by LIMK inhibition [9, 10, 16], by yet unknown mechanisms [3]. There are also evidences that LIMK may bind to and regulate other proteins [15, 52–54], so that other, known or yet unknown substrates may mediate antitumor effects of LIMK inhibition, independently of cofilin.

**Table 3. quantitative measurements of the phosphocofilin spots.** The data for spot I abundance are expressed in percentage of the sum of all spots measured on the silver-stained gels (see DOI: 10.5061/dryad.4n5929c for the complete gel images)The proteomic experiments have been carried out on four independent series for the human cell lines (1 to 4 in the table below) and on three independent series for the murine cell lines (1 to 3 in the table below).

| cell line | experimental series | Spot I ctrl | intensity pyr1 | ratio | paired T-test | unpaired T-test |
|---|---|---|---|---|---|---|
| MV4-11 | 1 | 0.3455 | 0.2257 | 0.6533 | 0.024 | 0.141 |
| | 2 | 0.2493 | 0.1444 | 0.5791 | | |
| | 3 | 0.1683 | 0.1412 | 0.8389 | | |
| | 4 | 0.1774 | 0.0796 | 0.4487 | | |
| | mean | 0.2351 | 0.1477 | | | |
| | ratio of means | | 0.6283 | | | |
| | mean of individual ratios | | 0.6283 | | | |
| Kasumi-1 | 1 | 0.1392 | 0.0856 | 0.6148 | 0.026 | 0.026 |
| | 2 | 0.3041 | 0.1099 | 0.3612 | | |
| | 3 | 0.2562 | 0.1523 | 0.5942 | | |
| | 4 | 0.2423 | 0.0789 | 0.3258 | | |
| | mean | 0.2355 | 0.1067 | | | |
| | ratio of means | | 0.4529 | | | |
| | mean of individual ratios | | 0.4740 | | | |
| 32D c-kit WT | 1 | 0.0881 | 0.0546 | 0.6195 | 0.080 | 0.121 |
| | 2 | 0.0787 | 0.0253 | 0.3211 | | |
| | 3 | 0.0420 | 0.02473 | 0.5891 | | |
| | mean | 0.0696 | 0.0348 | | | |
| | ratio of means | | 0.5009 | | | |
| | mean of individual ratios | | 0.5099 | | | |
| 32D c-kit D814V | 1 | 0.1364 | 0.0584 | 0.4279 | 0.0027 | 0.0054 |
| | 2 | 0.1311 | 0.0380 | 0.2896 | | |
| | 3 | 0.1062 | 0.0171 | 0.1606 | | |
| | mean | 0.1246 | 0.0378 | | | |
| | ratio of means | | 0.3034 | | | |
| | mean of individual ratios | | 0.2927 | | | |

Notes: the variability of some cultures (e.g. the MV 4–11 cell line) makes the unpaired T-test an unsuccessful approach to detect the significance of the decrease of the phosphocofilin spot brought by LIMK inhibition. The situation is even worse with the 32D- c-kit WT cell line where the inter-experiments variability is such that a 2-fold reduction does not reach the $p < 0.05$ cutoff
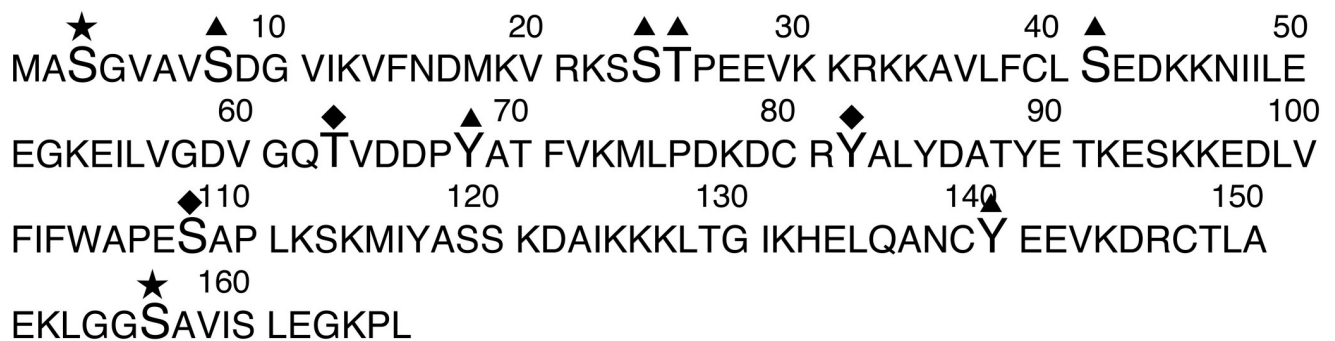
**Fig 4. Map of the cofilin phosphosites.** The phosphosites are displayed on the sequence of human cofilin. star: already known and described in the present study. triangles: described in the literature but not found in the present study. diamonds: described for the first time in the present study.

**Table 4. Quantitative measurements of the changes in phosphopeptide amounts brought by LIMK inhibition.**
The data are expressed in fold-changes in the phosphopeptides amounts in the phosphocofilin spot (control/pyr-1 treated). These fold-changes are obtained by the proper combination of the normalized phosphopeptide abundance described in S2–S5 Tables with the spot abundances changes described in Table 3.

| | Kasumi | MV4-11 | 32D c-kit WT | 32D c-kit D814V |
|---|---|---|---|---|
| S3 | 2.045 | 4.346 | 2.744 | 2.474 |
| T63a | 0.901 | 1.825 | 1.039 | 7.105 |
| T63b | 1.390 | 0.820 | ND | 2.548 |
| T63 sum | 1.502 | 1.422 | 1.039 | 5.202 |
| Y82 | 1.140 | 1.867 | 1.991 | 2.694 |
| S108 | 1.536 | 2.429 | ND | ND |
| S156 | 0.944 | 1.011 | 0.872 | 1.228 |

ND: modified peptide not detected. Note: as this quantitative analysis process is cumbersome. it has been carried out on one series of phosphocofilin spots (control vs. Pyr-1 treated) for each cell line

https://doi.org/10.1371/journal.pone.0208979.t004

Finally, our results show that cofilin is phosphorylated at other sites than S3, indicating that cofilin regulation is much more complex than expected. Such other phosphosites have already been described. For instance, it has been previously shown that phosphorylation at Y68 mediates protein degradation [55], while phosphorylation at S23-S24 is also implicated is the modulation of the actin severing function of cofilin and plays a role in cellular degradation [56]. We were not able to detect the Y68 phosphorylation. A plausible explanation is that such a phosphorylation, which impacts protein stability, can be expected to be transient and at a low level, and thus hardly detectable in our experimental conditions. Besides these known sites, we detected new phosphosites, both on tyrosine (Y82), threonine (T63) and serine (S108, S156), indicating that cofilin is a multi-regulated protein. The identification of the kinases responsible of these phosphorylations as well as their functional consequences should shed light on cofilin functions.

## Supporting information

**S1 Fig. Alignment for the detection of the cofilin spots.** A: Silver stained gel image (nonlinear 3–10 pH gradient).
B: India ink staining of a PVDF membrane blotted from an equivalent 2D gel.
C: Immunodetection of the cofilin spots on the membrane shown in B.
D: Immunodetection of the S3 phosphorylated cofilin spots on the membrane shown in B (image cropped on the cofilin region for space reasons).
Blue arrows: spots used to realign the 2D gel image and the stained blot image.
Purple solid lines: alignment of the cofilin spots not phosphorylated on S3.
Red dotted lines: alignment of the S3 phosphorylated cofilin spots.
X: spots detected as cofilin by blotting but not confirmed by mass spectrometry.
Red-circled spots: confirmed cofilin spots (detected by blotting and mass spectrometry.
Blue-circled spots: spots analyzed by mass spectrometry but not identified as cofilin.
Plus sign: Pyr-1 responsive S3 phosphorylated cofilin spot.
Note: the hand-made thick black dotted lines on the B panel were made on the membrane after the immunodetection process to point the major cofilin spots.
(JPG)

**S2 Fig. Annotated spectrum of the S3 phosphorylated peptide.** The annotated MS/MS spectrum of the peptide is shown at the bottom, with the assignment of the fragments on the top of the figure.
(JPG)

**S3 Fig. Annotated spectrum of the T63 phosphorylated peptide (mouse cofilin).** The annotated MS/MS spectrum of the peptide is shown at the bottom, with the assignment of the fragments on the top of the figure.
(JPG)

**S4 Fig. Annotated spectrum of the T63 phosphorylated peptide (human cofilin).** The annotated MS/MS spectrum of the peptide is shown at the bottom, with the assignment of the fragments on the top of the figure.
(JPG)

**S5 Fig. Annotated spectrum of the Y82 phosphorylated peptide.** The annotated MS/MS spectrum of the peptide is shown at the bottom, with the assignment of the fragments on the top of the figure.
(JPG)

**S6 Fig. Annotated spectrum of the S108 phosphorylated peptide.** The annotated MS/MS spectrum of the peptide is shown at the bottom, with the assignment of the fragments on the top of the figure.
(JPG)

**S7 Fig. Annotated spectrum of the S156 phosphorylated peptide.** The annotated MS/MS spectrum of the peptide is shown at the bottom, with the assignment of the fragments on the top of the figure.
(JPG)

**S1 Table. List of assigned peptides on the modified phosphocofilin spot (Kasumi-1 cell line, spot III).** The peptides identified by mass spectrometry are detailed in this table. Modified amino acids appear in lowercase in the peptide sequences, and the modifications are detailed in the corresponding column.
(XLSX)

**S2 Table. Peptide integration of the phosphocofilin spot, MV 4–11 cell line.** The peptides corresponding to all proteins detected in the phosphocofilin are quantified and summed in the control and pyr1-treated conditions. This summed is used to renormalize the intensities of the different peptides, and to calculate the relative peptide abundances at equal total protein mass.
(XLSX)

**S3 Table. Peptide integration of the phosphocofilin spot, Kasumi-1 cell line.** The peptides corresponding to all proteins detected in the phosphocofilin are quantified and summed in the control and pyr1-treated conditions. This summed is used to renormalize the intensities of the different peptides, and to calculate the relative peptide abundances at equal total protein mass.
(XLSX)

**S4 Table. Peptide integration of the phosphocofilin spot, 32D c-kit WT cell line.** The peptides corresponding to all proteins detected in the phosphocofilin are quantified and summed in the control and pyr1-treated conditions. This summed is used to renormalize the intensities of the different peptides, and to calculate the relative peptide abundances at equal total protein mass.
(XLSX)

**S5 Table. Peptide integration of the phosphocofilin spot, 32D c-kit D814V cell line.** The peptides corresponding to all proteins detected in the phosphocofilin are quantified and summed in the control and pyr1-treated conditions. This summed is used to renormalize the

intensities of the different peptides, and to calculate the relative peptide abundances at equal total protein mass.
(XLSX)

## Acknowledgments

## Author Contributions

**Conceptualization:** Renaud Prudent, Reuben Kapur, Fabrice Paublant, Laurence Lafanechère, Sarah Cianférani, Thierry Rabilloud.

**Data curation:** Sarah Cianférani, Thierry Rabilloud.

**Formal analysis:** Laurence Lafanechère, Thierry Rabilloud.

**Funding acquisition:** Fabrice Paublant, Sarah Cianférani, Thierry Rabilloud.

**Investigation:** Renaud Prudent, Nathalie Demoncheaux, Hélène Diemer, Véronique Collin-Faure, Thierry Rabilloud.

**Methodology:** Renaud Prudent, Nathalie Demoncheaux, Hélène Diemer, Véronique Collin-Faure, Thierry Rabilloud.

**Project administration:** Fabrice Paublant, Sarah Cianférani, Thierry Rabilloud.

**Supervision:** Renaud Prudent, Laurence Lafanechère, Sarah Cianférani.

**Validation:** Renaud Prudent, Sarah Cianférani, Thierry Rabilloud.

**Visualization:** Thierry Rabilloud.

**Writing – original draft:** Thierry Rabilloud.

**Writing – review & editing:** Renaud Prudent, Nathalie Demoncheaux, Hélène Diemer, Véronique Collin-Faure, Reuben Kapur, Fabrice Paublant, Laurence Lafanechère, Sarah Cianférani.

## References

1. Dumontet C, Jordan MA. Microtubule-binding agents: a dynamic field of cancer therapeutics. Nat Rev Drug Discov. 2010; 9(10):790–803. https://doi.org/10.1038/nrd3253 PMID: 20885410

2. Stehn JR, Haass NK, Bonello T, Desouza M, Kottyan G, Treutlein H, et al. A novel class of anticancer compounds targets the actin cytoskeleton in tumor cells. Cancer Res. 2013; 73(16):5169–82 https://doi.org/10.1158/0008-5472.CAN-12-4501 PMID: 23946473

3. Prunier C, Prudent R, Kapur R, Sadoul K, Lafanechere L. LIM kinases: cofilin and beyond. Oncotarget. 2017; 8(25):41749–63. https://doi.org/10.18632/oncotarget.16978 PMID: 28445157

4. Manetti F. LIM kinases are attractive targets with many macromolecular partners and only a few small molecule regulators. Medicinal Research Reviews. 2012; 32(5):968–98. https://doi.org/10.1002/med.20230 PMID: 22886629

5. Wang W, Eddy R, Condeelis J. The cofilin pathway in breast cancer invasion and metastasis. Nat Rev Cancer. 2007; 7(6):429–40. https://doi.org/10.1038/nrc2148 PMID: 17522712

6. Van Troys M, Huyck L, Leyman S, Dhaese S, Vandekerkhove J, Ampe C. Ins and outs of ADF/cofilin activity and regulation. Eur J Cell Biol. 2008; 87(8–9):649–67. https://doi.org/10.1016/j.ejcb.2008.04.001 PMID: 18499298

7. Yang N, Higuchi O, Ohashi K, Nagata K, Wada A, Kangawa K, et al. Cofilin phosphorylation by LIM-kinase 1 and its role in Rac-mediated actin reorganization. Nature. 1998; 393(6687):809–12. https://doi.org/10.1038/31735 PMID: 9655398

8. Lindstrom NO, Neves C, McIntosh R, Miedzybrodzka Z, Vargesson N, Collinson JM. Tissue specific characterisation of Lim-kinase 1 expression during mouse embryogenesis. Gene Expr Patterns. 2011; 11(3–4):221–32. https://doi.org/10.1016/j.gep.2010.12.003 PMID: 21167960

9. Mardilovich K, Baugh M, Crighton D, Kowalczyk D, Gabrielsen M, Munro J, et al. LIM kinase inhibitors disrupt mitotic microtubule organization and impair tumor cell proliferation. Oncotarget. 2015; 6 (36):38469–86. https://doi.org/10.18632/oncotarget.6288 PMID: 26540348

10. Prudent R, Vassal-Stermann E, Nguyen CH, Pillet C, Martinez A, Prunier C, et al. Pharmacological Inhibition of LIM Kinase Stabilizes Microtubules and Inhibits Neoplastic Growth. Cancer Research. 2012; 72(17):4429–39. https://doi.org/10.1158/0008-5472.CAN-11-3342 PMID: 22761334

11. Nakashima S, Matsuda H, Kurume A, Oda Y, Nakamura S, Yamashita M, et al. Cucurbitacin E as a new inhibitor of cofilin phosphorylation in human leukemia U937 cells. Bioorg Med Chem Lett. 2010; 20 (9):2994–7. https://doi.org/10.1016/j.bmcl.2010.02.062 PMID: 20347305

12. Ohashi K, Sampei K, Nakagawa M, Uchiumi N, Amanuma T, Aiba S, et al. Damnacanthal, an effective inhibitor of LIM-kinase, inhibits cell migration and invasion. Molecular Biology of the Cell. 2015; 25 (6):828–40.

13. Sari-Hassoun M, Clement MJ, Hamdi I, Bollot G, Bauvais C, Joshi V, et al. Cucurbitacin I elicits the formation of actin/phospho-myosin II co-aggregates by stimulation of the RhoA/ROCK pathway and inhibition of LIM-kinase. Biochemical Pharmacology. 2016; 102:45–63. https://doi.org/10.1016/j.bcp.2015.12.013 PMID: 26707799

14. Prunier C, Josserand V, Vollaire J, Beerling E, Petropoulos C, Destaing O, et al. LIM Kinase Inhibitor Pyr1 Reduces the Growth and Metastatic Load of Breast Cancers. Cancer Research. 2016; 76 (12):3541–52. https://doi.org/10.1158/0008-5472.CAN-15-1864 PMID: 27216191

15. Lagoutte E, Villeneuve C, Lafanechere L, Wells CM, Jones GE, Chavrier P, et al. LIMK Regulates Tumor-Cell Invasion and Matrix Degradation Through Tyrosine Phosphorylation of MT1-MMP. Scientific Reports. 2016; 6: 24925 https://doi.org/10.1038/srep24925 PMID: 27116935

16. Prunier C, Kapur R, Lafanechere L. Targeting LIM kinases in taxane resistant tumors. Oncotarget. 2016; 7(32):50816–7. https://doi.org/10.18632/oncotarget.10816 PMID: 27463010

17. Mali RS, Kapur R. Targeting Rho associated kinases in leukemia and myeloproliferative neoplasms. Oncotarget. 2012; 3(9):909–10. https://doi.org/10.18632/oncotarget.664 PMID: 23006984

18. Kapur R, Shi J, Ghosh J, Munugalavadla V, Sims E, Martin H, et al. ROCK1 via LIM kinase regulates growth, maturation and actin based functions in mast cells. Oncotarget. 2016; 7(13):16936–47. https://doi.org/10.18632/oncotarget.7851 PMID: 26943578

19. Guo H, Gu F, Li W, Zhang B, Niu R, Fu L, et al. Reduction of protein kinase C zeta inhibits migration and invasion of human glioblastoma cells. J Neurochem. 2009; 109(1):203–13. https://doi.org/10.1111/j.1471-4159.2009.05946.x PMID: 19187446

20. Heidebrecht F, Heidebrecht A, Schulz I, Behrens SE, Bader A. Improved semiquantitative Western blot technique with increased quantification range. J Immunol Methods. 2009; 345(1–2):40–8. https://doi.org/10.1016/j.jim.2009.03.018 PMID: 19351538

21. Charette SJ, Lambert H, Nadeau PJ, Landry J. Protein quantification by chemiluminescent Western blotting: elimination of the antibody factor by dilution series and calibration curve. J Immunol Methods. 2010; 353(1–2):148–50. https://doi.org/10.1016/j.jim.2009.12.007 PMID: 20035759

22. Eaton SL, Roche SL, Llavero Hurtado M, Oldknow KJ, Farquharson C, Gillingwater TH, et al. Total protein analysis as a reliable loading control for quantitative fluorescent Western blotting. PLoS One. 2013; 8(8):e72457. https://doi.org/10.1371/journal.pone.0072457 PMID: 24023619

23. Ghosh R, Gilda JE, Gomes AV. The necessity of and strategies for improving confidence in the accuracy of western blots. Expert Rev Proteomics. 2014; 11(5):549–60. https://doi.org/10.1586/14789450.2014.939635 PMID: 25059473

24. Triboulet S, Aude-Garcia C, Carriere M, Diemer H, Proamer F, Habert A, et al. Molecular responses of mouse macrophages to copper and copper oxide nanoparticles inferred from proteomic analyses. Mol Cell Proteomics. 2013; 12:3108–22 https://doi.org/10.1074/mcp.M113.030742 PMID: 23882024

25. Bradford MM. A rapid and sensitive method for the quantitation of microgram quantities of protein utilizing the principle of protein-dye binding. Anal Biochem. 1976; 72:248–54. PMID: 942051

26. Gianazza E, Celentano F, Magenes S, Ettori C, Righetti PG. Formulations for immobilized pH gradients including pH extremes. Electrophoresis. 1989; 10(11):806–8. https://doi.org/10.1002/elps.1150101115 PMID: 2612482

**27.** Rabilloud T, Valette C, Lawrence JJ. Sample application by in-gel rehydration improves the resolution of two-dimensional electrophoresis with immobilized pH gradients in the first dimension. Electrophoresis. 1994; 15(12):1552–8. PMID: 7536671

**28.** Luche S, Diemer H, Tastet C, Chevallet M, Van Dorsselaer A, Leize-Wagner E, et al. About thiol derivatization and resolution of basic proteins in two-dimensional electrophoresis. Proteomics. 2004; 4 (3):551–61. https://doi.org/10.1002/pmic.200300589 PMID: 14997479

**29.** Gorg A, Postel W, Weser J, Gunther S, Strahler JR, Hanash SM, et al. Elimination of Point Streaking on Silver Stained Two-Dimensional Gels by Addition of Iodoacetamide to the Equilibration Buffer. Electrophoresis. 1987; 8(2):122–4.

**30.** Tastet C, Lescuyer P, Diemer H, Luche S, van Dorsselaer A, Rabilloud T. A versatile electrophoresis system for the analysis of high- and low-molecular-weight proteins. Electrophoresis. 2003; 24 (11):1787–94. https://doi.org/10.1002/elps.200305400 PMID: 12783456

**31.** Chevallet M, Luche S, Rabilloud T. Silver staining of proteins in polyacrylamide gels. Nat Protoc. 2006; 1(4):1852–8. https://doi.org/10.1038/nprot.2006.288 PMID: 17487168

**32.** Kyhse-Andersen J. Electroblotting of multiple gels: a simple apparatus without buffer tank for rapid transfer of proteins from polyacrylamide to nitrocellulose. J Biochem Biophys Methods. 1984; 10(3–4):203–9. PMID: 6530509

**33.** Lauriere M. A semidry electroblotting system efficiently transfers both high- and low-molecular-weight proteins separated by SDS-PAGE. Anal Biochem. 1993; 212(1):206–11. https://doi.org/10.1006/abio.1993.1313 PMID: 8368495

**34.** Eynard L, Lauriere M. The combination of Indian ink staining with immunochemiluminescence detection allows precise identification of antigens on blots: application to the study of glycosylated barley storage proteins. Electrophoresis. 1998; 19(8–9):1394–6. https://doi.org/10.1002/elps.1150190833 PMID: 9694288

**35.** Gharahdaghi F, Weinberg CR, Meagher DA, Imai BS, Mische SM. Mass spectrometric identification of proteins from silver-stained polyacrylamide gel: A method for the removal of silver ions to enhance sensitivity. Electrophoresis. 1999; 20(3):601–5. https://doi.org/10.1002/(SICI)1522-2683(19990301)20:3<601::AID-ELPS601>3.0.CO;2-6 PMID: 10217175

**36.** Richert S, Luche S, Chevallet M, Van Dorsselaer A, Leize-Wagner E, Rabilloud T. About the mechanism of interference of silver staining with peptide mass spectrometry. Proteomics. 2004; 4(4):909–16. https://doi.org/10.1002/pmic.200300642 PMID: 15048973

**37.** Vizcaino JA, Csordas A, Del-Toro N, Dianes JA, Griss J, Lavidas I, et al. 2016 update of the PRIDE database and its related tools. Nucleic Acids Res. 2016; 44(22):11033. https://doi.org/10.1093/nar/gkw880 PMID: 27683222

**38.** Schilling B, Rardin MJ, MacLean BX, Zawadzka AM, Frewen BE, Cusack MP, et al. Platform-independent and label-free quantitation of proteomic data using MS1 extracted ion chromatograms in skyline: application to protein acetylation and phosphorylation. Mol Cell Proteomics. 2012; 11(5):202–14. https://doi.org/10.1074/mcp.M112.017707 PMID: 22454539

**39.** Nick HJ, Kim HG, Chang CW, Harris KW, Reddy V, Klug CA. Distinct classes of c-Kit-activating mutations differ in their ability to promote RUNX1-ETO-associated acute myeloid leukemia. Blood. 2012; 119 (6):1522–31. https://doi.org/10.1182/blood-2011-02-338228 PMID: 21937700

**40.** Chatterjee A, Ghosh J, Kapur R. Mastocytosis: a mutated KIT receptor induced myeloproliferative disorder. Oncotarget. 2015; 6(21):18250–64. https://doi.org/10.18632/oncotarget.4213 PMID: 26158763

**41.** Huyck L, Van Troys M, Ampe C. Phosphosite conservation in single domain orthologs versus paralogs: a way to combine differential regulation with redundant core functions. FEBS Lett. 2012; 586(4):296–302. https://doi.org/10.1016/j.febslet.2012.01.018 PMID: 22265693

**42.** Speicher KD, Kolbas O, Harper S, Speicher DW. Systematic analysis of peptide recoveries from in-gel digestions for protein identifications in proteome studies. J Biomol Tech. 2000; 11(2):74–86. PMID: 19499040

**43.** Wang W, Mouneimne G, Sidani M, Wyckoff J, Chen X, Makris A, et al. The activity status of cofilin is directly related to invasion, intravasation, and metastasis of mammary tumors. J Cell Biol. 2006; 173 (3):395–404. https://doi.org/10.1083/jcb.200510115 PMID: 16651380

**44.** Sidani M, Wessels D, Mouneimne G, Ghosh M, Goswami S, Sarmiento C, et al. Cofilin determines the migration behavior and turning frequency of metastatic cancer cells. J Cell Biol. 2007; 179(4):777–91. https://doi.org/10.1083/jcb.200707009 PMID: 18025308

**45.** Shibue T, Brooks MW, Weinberg RA. An integrin-linked machinery of cytoskeletal regulation that enables experimental tumor initiation and metastatic colonization. Cancer Cell. 2013; 24(4):481–98. https://doi.org/10.1016/j.ccr.2013.08.012 PMID: 24035453

**46.** Fife CM, McCarroll JA, Kavallaris M. Movers and shakers: cell cytoskeleton in cancer metastasis. Br J Pharmacol. 2014; 171(24):5507–23. https://doi.org/10.1111/bph.12704 PMID: 24665826

**47.** Scott RW, Hooper S, Crighton D, Li A, Konig I, Munro J, et al. LIM kinases are required for invasive path generation by tumor and tumor-associated stromal cells. Journal of Cell Biology. 2010; 191(1):169–85. https://doi.org/10.1083/jcb.201002041 PMID: 20876278

**48.** Nakano K, Kanai-Azuma M, Kanai Y, Moriyama K, Yazaki K, Hayashi Y, et al. Cofilin phosphorylation and actin polymerization by NRK/NESK, a member of the germinal center kinase family. Exp Cell Res. 2003; 287(2):219–27. PMID: 12837278

**49.** Toshima J, Toshima JY, Takeuchi K, Mori R, Mizuno K. Cofilin phosphorylation and actin reorganization activities of testicular protein kinase 2 and its predominant expression in testicular Sertoli cells. J Biol Chem. 2001; 276(33):31449–58. https://doi.org/10.1074/jbc.M102988200 PMID: 11418599

**50.** Ritchey L, Chakrabarti R. Aurora A kinase modulates actin cytoskeleton through phosphorylation of Cofilin: Implication in the mitotic process. Biochim Biophys Acta. 2014; 1843(11):2719–29. https://doi.org/10.1016/j.bbamcr.2014.07.014 PMID: 25090971

**51.** Li R, Doherty J, Antonipillai J, Chen S, Devlin M, Visser K, et al. LIM kinase inhibition reduces breast cancer growth and invasiveness but systemic inhibition does not reduce metastasis in mice. Clinical & Experimental Metastasis. 2013; 30(4):483–95.

**52.** Yang EJ, Yoon JH, Min DS, Chung KC. LIM kinase 1 activates cAMP-responsive element-binding protein during the neuronal differentiation of immortalized hippocampal progenitor cells. J Biol Chem. 2004; 279(10):8903–10. https://doi.org/10.1074/jbc.M311913200 PMID: 14684741

**53.** Liao Q, Li R, Zhou R, Pan ZH, Xu LJ, Ding YQ, et al. LIM kinase 1 interacts with myosin-9 and alpha-actinin-4 and promotes colorectal cancer progression. British Journal of Cancer. 2017; 117(4):563–71. https://doi.org/10.1038/bjc.2017.193 PMID: 28664914

**54.** Ou S, Tan MH, Weng T, Li H, Koh CG. LIM kinase1 regulates mitotic centrosome integrity via its activity on dynein light intermediate chains. Open Biol. 2018; 8(6): pii:170202 https://doi.org/10.1098/rsob.170202 PMID: 29925632

**55.** Yoo Y, Ho HJ, Wang C, Guan JL. Tyrosine phosphorylation of cofilin at Y68 by v-Src leads to its degradation through ubiquitin-proteasome pathway. Oncogene. 2010; 29(2):263–72. https://doi.org/10.1038/onc.2009.319 PMID: 19802004

**56.** Sakuma M, Shirai Y, Yoshino K, Kuramasu M, Nakamura T, Yanagita T, et al. Novel PKCalpha-mediated phosphorylation site(s) on cofilin and their potential role in terminating histamine release. Mol Biol Cell. 2012; 23(18):3707–21. https://doi.org/10.1091/mbc.E12-01-0053 PMID: 22855535